Mass spectra, Regge trajectories and decay properties of heavy-flavour mesons

Rahulbhai Mistry[a,*], Manan Shah[b], and Ajay Majethiya[a]

[a]*Department of Physics, V. S. Patel College of Arts and Science, Veer Narmad South Gujarat University, Surat, 395007, Gujarat, India.*
**e-mail: mistrirahul24@gmail.com*
[b]*P. D. Patel Institute of Applied Sciences, CHARUSAT Campus, Off. Nadiad-Petlad Road, Changa, 388421, Gujarat, India.*

Received 27 June 2023; accepted 17 August 2023

In this article, we study the mass spectra, Regge trajectories and decay properties of heavy-flavour mesons $Q\bar{Q}$ $(Q = c, b)$ within a non-relativistic quark model. The spin hyperfine interaction is used to get the prediction for the heavy-meson masses for radial and orbital excitations. By using the radial and orbital excitations, we construct Regge trajectories for the heavy-mesons in the (J, M^2) and (n, M^2) plane and find their slopes and intercepts. We have computed leptonic, photonic and gluonic decay widths of heavy flavour mesons with and without QCD correction factor. We have compared our results of masses as well as decay widths with other theoretical and lattice QCD predictions for each states. Moreover, the known experimental results are also reasonably close to our predicted results.

Keywords: Hadron spectroscopy; hadron structure; phenomenological approaches to hadron physics.

DOI: https://doi.org/10.31349/RevMexFis.70.010801

1. Introduction

Heavy-flavour mesons $Q\bar{Q}$ $(Q \in \{c, b\})$; the bound states of heavy quark and it's anti-quark are best tools for understanding of the strong interactions. In 1974, the J/ψ particle was discovered experimentally [1,2], which is identified as bound states of charm(c) and its anti-particle ($\bar{c}$) [3]. In 1977, bottomonium $(b\bar{b})$ was discovered experimentally as spin-triplet states $\Upsilon(1S), \Upsilon(2S)$ and $\Upsilon(3S)$. [4,5]. Since then in the past few years remarkable experimental progress has been made in the field of heavy quarkonium physics due to the available experimental facilities such as LHCb, Belle, BABAR, CDF, BESIII and CLEOc etc., which has opened up new challenges and opportunities in the theoretical understanding of hadrons containing heavy flavour quarks.

Large amount of data is available for masses along with different decay modes in recent PDG [6]. In heavy flavor spectroscopy mesons have been observed; experimentally and studied by theoretical approaches like lattice QCD, QCD sum rules, Non-Relativistic QCD, some relativistic and non-relativistic potential models to explain the static and dynamics properties of these states. Thus, to understand the newly observed states in the heavy sector; study of the mass spectra and decay properties of heavy mesons become very important for the better understanding of quark-antiquark dynamics and QCD within the $Q\bar{Q}$ bound states. In hadron physics The quark-antiquark interacting potential require the understanding of strong interactions. Different potential models may predicted similar mass spectra matching with experimental results but it's important to have mutual agreement of mass spectra along with decay properties such as leptonic, photonic and gluonic decays. Study of decay properties of quarkonia $(Q\bar{Q})$ decays into leptons, photons and gluons is very important for the identification of resonances as well as to recognize conventional and exotic structure [7,8]. So, apart from the successful predictions of the masses, validity and relaiability of any potential model depends also on the successful predictions of their decay properties.

After the brief introduction in Sec. 1, the paper is arranged as follows. In Sec. 2 we present the theoretical framework for the mass spectra and decays of heavy-flavor mesons $(Q\bar{Q})$ into leptons, photons and gluons. In Sec. 3, we discuss results and draw our conclusions.

2. Theoretical framework

To study the mass spectra of heavy-flavour mesons such as charmonium $(c\bar{c})$ and bottomonium $(b\bar{b})$ as a bound states system of quark-antiquark $(Q\bar{Q})$, within a non-relativistic quark model; we have considered a non-relativistic Hamiltonian for two body problem expressed as

$$H = \sum_{i=1}^{2} m_i + \frac{-\hbar^2}{2m_i}\nabla^2 + V(r). \tag{1}$$

In heavy-flavour quark-antiquark bound states system the kinetic energy of the quarks is smaller than the rest mass energy, Thus, a non-relativistic treatment with static potential could provide an effective approximation. To solve the two body problem within a non-relativistic framework we have considered the time-independent Schrodinger equation;

$$\left[\frac{1}{2\mu}\left(-\frac{d^2}{dr^2} + \frac{l(l+1)}{r^2}\right) + V_{Q\bar{Q}}(r)\right]\psi(r) = E\psi(r). \tag{2}$$

We have considered the quark-antiquark interaction potential based on QCD, which is color Coulomb plus confining power

law potential responsible for the asymptotic freedom and the color confinement phenomenon given by [9, 10]

$$V_{Q\bar{Q}}(r) = V_V + V_S = \frac{\alpha}{r} + br^p, \tag{3}$$

where α is couling strength, b is string tension related to strength of confinement, p is the potential exponent that we vary from 0.1 to 2.0. To solve the Schrodinger equation we have used variational method with hydrogenic radial wave function for the (n,l) states. spin dependent interaction potential $V_{SD}(r)$, sum of spin-spin (V_{ss}), spin-orbit (V_{LS}) and tensor (V_T) iteraction potential as a perturbative correction account for especially in excited states. All the three spin-dependent interaction terms are driven by the Breit-Fermi Hamiltonian for one-gluon exchange given by [11].

$$V_{SS}(r) = C_{SS}(r) S_1 \cdot S_2, \tag{4}$$

$$V_{LS}(r) = C_{LS}(r) L \cdot S, \tag{5}$$

$$V_T(r) = C_T(r) \left(\frac{(S_1 \cdot r)(S_2 \cdot r)}{r^2} - \frac{1}{3}(S_1 \cdot S_2) \right), \tag{6}$$

where S_1 and S_2 are the spins of particle 1 and 2 respectively, and S is the total spin in our consideration and radial dependent coefficient come from the vector $V_V(r)$ and scalar $V_S(r)$ part of the potential in Eq. (2);

$$C_{SS}(r) = \frac{2}{3m^2} \nabla^2 V_V(r), \tag{7}$$

$$C_{LS}(r) = \frac{1}{2m^2} \frac{1}{r} \left[3\frac{dV_V(r)}{dr} - \frac{dV_S(r)}{dr} \right], \tag{8}$$

$$C_T(r) = \frac{1}{m^2} \left[\frac{1}{r} 3\frac{dV_V(r)}{dr} - \frac{d^2V_V(r)}{dr^2} \right] \tag{9}$$

After solving the Schrodinger equation with quark-antiquark interaction potential the masses of particular states of heavy-flavour mesons $Q\bar{Q}$ are computed as,

$$M_{Q\bar{Q}} = m_Q + m_{\bar{Q}} + E_{Q\bar{Q}} + \langle V_{SD} \rangle_{Q\bar{Q}}, \tag{10}$$

where m_Q and $m_{\bar{Q}}$ are the masses of quark and antiquark respectively, $E_{Q\bar{Q}}$ represent the binding energy of quark-antiquark system. V_{SD} is the spin dependent interactions. The parity and charge cojugation quantum numbers of $Q\bar{Q}$ states are given by $P = (-1)^{L+1}$ and $C = (-1)^{L+S}$ respectively, where L is the relative orbital angular momentum and S is the total spin of the bound states.

Decays of heavy-flavour mesons into leptons, photons or gluons is very useful to study the decay properties of mesons($Q\bar{Q}$) as well as for the prediction and identification of resonance. It can also helpful to identify conventional and exotic structure of mesons [7]. By using the masses of quarkonia we also computed decay rate of leptonic, photonic and gluonic decays of $Q\bar{Q}$ states.

The Leptonic decay of n^3S_1 states annihilate into lepton pair leads to decay $J/\psi \to e^+e^-$ and $\Upsilon \to e^+e^-$, hence decay rate is given by [7, 12, 13]

$$\Gamma^{e^+e^-} = \Gamma(n^3S_1 \to e^+e^-) = \frac{4{e_Q}^2\alpha^2|R_{nl}(0)|^2}{M_{nS}^2}, \tag{11}$$

$$\begin{aligned}\Gamma_{cf}^{e^+\,e^-} &= \Gamma_{cf}((n^3S_1 \to e^+e^-) \\ &= \frac{4{e_Q}^2\alpha^2|R_{nl}(0)|^2}{M_{nS}^2} \left(1 - \frac{16\alpha_s}{3\pi}\right),\end{aligned} \tag{12}$$

where M_{nS} is mass of the decaying corresponding $(Q\bar{Q})$ states. $\Gamma^{e^+e^-}$ and $\Gamma_{cf}^{e^+\,e^-}$ are the decay rate without and with radiative quantum chromo-dynamics correction factor respectively.

The photonic decay of n^1S_0 and n^3S_1 states annihilate into two and three photon leads to the decays $\eta_c \to \gamma\gamma$ $\eta_b \to \gamma\gamma$, $J/\psi \to 3\gamma$ and $\upsilon \to 3\gamma$, hence the annihilation decay rate of charmonium $(c\bar{c})$ and bottomonium into two or three photons with and without quantum chromo-dynamics correction factor is given by [7, 12]

$$\Gamma^{\gamma\gamma} = \Gamma(n^1S_0 \to \gamma\gamma) = \frac{3Q^4\alpha^2|R_{nl}(0)|^2}{M_{nS}^2}, \tag{13}$$

$$\begin{aligned}\Gamma_{cf}^{\gamma\gamma} &= \Gamma_{cf}(n^1S_0 \to \gamma\gamma) \\ &= \frac{3Q^4\alpha^2|R_{nl}(0)|^2}{M_{nS}^2} \left(1 - \frac{3.4\alpha_s}{\pi}\right),\end{aligned} \tag{14}$$

$$\Gamma^{3\gamma} = \Gamma(n^3S_1 \to 3\gamma) = \frac{4(\pi^2-9)e_Q^6\alpha^3|R_{nl}(0)|^2}{3\pi M_{nS}^2}, \tag{15}$$

$$\begin{aligned}\Gamma_{cf}^{3\gamma} &= \Gamma_{cf}(n^3S_1 \to 3\gamma) \\ &= \frac{4(\pi^2-9)e_Q^6\alpha^3|R_{nl}(0)|^2}{3\pi M_{nS}^2} \left(1 - \frac{12.6\alpha_s}{\pi}\right).\end{aligned} \tag{16}$$

The gluonic decay of n^1S_0 and n^3S_1 states decay into two or three gluons as well as into gluon with photon leads to decay $\eta_c \to gg, \eta_b \to gg, J/\psi \to 3g$ and $\Upsilon \to \gamma gg$. hence the gluonic decay rate with and without radiative quantum chromo-dynamics correction factor is given by [7, 12, 14]

$$\Gamma^{gg} = \Gamma(n^1S_0 \to gg) = \frac{2\alpha_s^2|R_{nl}(0)|^2}{3M_{nS}^2}, \tag{17}$$

$$\begin{aligned}\Gamma_{cf}^{gg} &= \Gamma_{cf}(n^1S_0 \to gg) \\ &= \frac{2\alpha_s^2|R_{nl}(0)|^2}{3M_{nS}^2} \left(1 + \frac{4.4\alpha_s}{\pi}\right),\end{aligned} \tag{18}$$

$$\Gamma^{3g} = \Gamma(n^3S_1 \to 3g) = \frac{10(\pi^2-9)\alpha_s^3|R_{nl}(0)|^2}{81\pi M_{nS}^2}, \tag{19}$$

$$\begin{aligned}\Gamma_{cf}^{3g} &= \Gamma_{cf}(n^3S_1 \to 3g) \\ &= \frac{10(\pi^2-9)\alpha_s^3|R_{nl}(0)|^2}{81\pi M_{nS}^2} \left(1 - \frac{6.6\alpha_s}{\pi}\right),\end{aligned} \tag{20}$$

TABLE I. Potential-model parameters for the present work.

	$m_Q = m_{\bar{Q}}$ (GeV)	M_{SA} (GeV)	α_s (GeV)
$c\bar{c}$	1.31	3.068	0.40
$b\bar{b}$	4.66	9.445	0.30

TABLE II. S-wave masses of pseudoscalar (η_c) and vector meson (J/ψ).

states	power index (p)	$R_{nl}(0)$ (GeV$^{3/2}$)	η_c n^1S_0 (GeV)	J/ψ n^3S_1 (GeV)
	0.1	0.560	3.041	3.077
	0.5	0.948	3.006	3.088
1S	1.0	1.255	2.975	3.097
	1.5	1.412	2.958	3.103
	2.0	1.549	2.944	3.108
	[6]		2.980	3.097
	[15]		2.983	3.075
	[17]		2.980	3.097
	0.1	0.332	3.200	3.210
	0.5	0.878	3.419	3.451
2S	1.0	1.425	3.643	3.690
	1.5	1.835	3.814	3.869
	2.0	2.159	3.935	3.996
	[6]		3.639	3.686
	[15]		3.623	3.664
	[17]		3.597	3.686
	0.1	0.279	3.255	3.260
	0.5	0.923	3.647	3.662
3S	1.0	1.645	4.107	4.129
	1.5	2.291	4.495	4.524
	2.0	2.803	4.800	4.835
	[6]			4.039
	[15]		4.046	4.073
	[17]		4.014	4.095
	0.1	0.256	3.287	3.290
	0.5	0.947	3.814	3.822
4S	1.0	1.875	4.490	4.505
	1.5	2.778	5.108	5.131
	2.0	3.331	5.642	5.670
	[6]			4.421
	[15]		4.395	4.417

$$\Gamma^{\gamma gg} = \Gamma(n^3S_1 \to \gamma gg) = \frac{8(\pi^2-9)e_Q^2\alpha\alpha_s^2|R_{nl}(0)|^2}{9\pi M_{nS}^2}, \quad (21)$$

$$\Gamma^{\gamma gg}_{cf} = \Gamma_{cf}(n^3S_1 \to \gamma gg) = \frac{8(\pi^2-9)e_Q^2\alpha\alpha_s^2|R_{nl}(0)|^2}{9\pi M_{nS}^2}\left(1-\frac{4.4\alpha_s}{\pi}\right), \quad (22)$$

where the subscripts "cf" represent the decay rate with radiative quantum chromo-dynamics correction factor.

3. Results, summary and discussion

3.1. Mass Spectra

To study the mass spectra of heavy-flavour mesons in the framework of non-relativistic quark model, we have used color coulomb plus confining power law potential. To get the experimental ground states centre of weight or spin average masses of $c\bar{c}$ and $b\bar{b}$ which are computed from the respective known experimental masses (taken from recent PDG [6]) of

TABLE III. P-wave masses of charmonium $c\bar{c}$.

states	power index (p)	$R_{nl}(0)$ (GeV$^{3/2}$)	n^3P_0 (GeV)	n^3P_1 (GeV)	n^1P_1 (GeV)	n^3P_2 (GeV)
	0.1	0.079	3.500	3.508	3.512	3.518
	0.5	0.315	3.459	3.495	3.508	3.534
1P	1.0	0.554	3.413	3.481	3.505	3.556
	1.5	0.726	3.372	3.467	3.500	3.574
	2.0	0.793	3.357	3.463	3.499	3.581
	[6]		3.414	3.510	3.525	3.556
	[15]		3.410	3.492	3.502	3.543
	[17]		3.416	3.508	3.527	3.558
	0.1	0.026	3.578	3.584	3.587	3.592
	0.5	0.145	3.720	3.766	3.784	3.822
2P	1.0	0.309	3.821	3.935	3.981	4.076
	1.5	0.468	3.858	4.048	4.127	4.283
	2.0	0.605	3.856	4.115	4.227	4.438
	[6]					3.927
	[15]		3.846	3.922	3.930	3.969
	[17]		3.844	3.894	3.960	3.994
	0.1	0.013	3.625	3.630	3.633	3.637
	0.5	0.087	3.908	3.961	3.984	4.029
3P	1.0	0.212	4.140	4.298	4.372	4.498
	1.5	0.347	4.264	4.549	4.691	4.912
	2.0	0.455	4.343	4.737	4.940	5.239
	[15]		4.205	4.276	4.286	4.324

TABLE IV. D-wave masses charmonium $c\bar{c}$.

states	power index (p)	$R_{nl}(0)$ (GeV$^{3/2}$)	n^3D_1 (GeV)	n^3D_2 (GeV)	n^1D_2 (GeV)	n^3D_3 (GeV)
	0.1	0.009	3.775	3.777	3.778	3.779
	0.5	0.079	3.772	3.776	3.777	3.779
1D	1.0	0.186	3.772	3.778	3.777	3.779
	1.5	0.286	3.768	3.778	3.776	3.780
	2.0	0.365	3.763	3.777	3.775	3.783
	[6]		3.773			
	[15]		3.778	3.792	3.791	3.797
	0.1	0.003	3.834	3.835	3.836	3.837
	0.5	0.034	4.002	4.012	4.014	4.023
2D	1.0	0.097	4.169	4.194	4.197	4.219
	1.5	0.162	4.297	4.336	4.340	4.376
	2.0	0.218	4.401	4.450	4.454	4.500

TABLE V. S-wave masses of pseudoscalar (η_b) and vector meson Υ.

states	power index (p)	$R_{nl}(0)$ (GeV$^{3/2}$)	η_b n^1S_0 (GeV)	Υ n^3S_1 (GeV)
	0.1	1.986	9.421	9.453
	0.5	2.642	9.405	9.458
1S	1.0	3.203	9.390	9.463
	1.5	3.560	9.380	9.467
	2.0	3.820	9.372	9.469
	[6]		9.393	9.460
	[16]		9.409	9.440
	[17]		9.414	9.461
	0.1	0.931	9.625	9.631
	0.5	2.015	9.784	9.806
2S	1.0	3.207	9.959	9.999
	1.5	4.123	10.09	10.15
	2.0	4.809	10.20	10.26
	[6]		–	10.02
	[16]		9.987	9.997
	[17]		9.999	10.02
	0.1	0.684	9.678	9.682
	0.5	1.940	9.963	9.977
3S	1.0	3.564	10.32	10.35
	1.5	5.053	10.64	10.68
	2.0	6.108	10.91	10.95
	[6]		–	10.35
	[16]		10.32	10.33
	[17]		10.34	10.36
	0.1	0.583	9.706	9.708
	0.5	1.977	10.08	10.09
4S	1.0	3.934	10.06	10.63
	1.5	5.956	11.13	11.15
	2.0	7.424	11.59	11.61
	[6]		–	10.58
	[16]		10.59	10.60

TABLE VI. P-wave masses of bottomonium $b\bar{b}$.

states	power index (p)	$R_{nl}(0)$ (GeV$^{3/2}$)	n^3P_0 (GeV)	n^3P_1 (GeV)	n^1P_1 (GeV)	n^3P_2 (GeV)
	0.1	0.428	9.891	9.894	9.897	9.899
	0.5	1.335	9.876	9.889	9.896	9.906
1P	1.0	2.205	9.860	9.884	9.896	9.913
	1.5	2.898	9.845	9.879	9.895	9.920
	2.0	3.316	9.835	9.875	9.894	9.924
	[6]		9.859	9.892	9.899	9.912
	[16]		9.863	9.893	9.898	9.915
	[17]		9.900	9.861	9.891	9.912
	0.1	0.118	9.967	9.969	9.970	9.72
	0.5	0.564	10.10	10.11	10.12	10.14
2P	1.0	1.163	10.23	10.26	10.28	10.30
	1.5	1.667	10.32	10.38	10.40	10.45
	2.0	2.121	10.39	10.46	10.49	10.55
	[6]		10.23	10.26	-	10.27
	[16]		10.21	10.23	10.24	10.26
	[17]		10.26	10.23	10.25	10.27
	0.1	0.052	10.00	10.01	10.01	10.02
	0.5	0.322	10.26	10.28	10.29	10.30
3P	1.0	0.766	10.52	10.57	10.59	10.63
	1.5	1.272	10.73	10.81	10.84	10.92
	2.0	1.699	10.88	10.99	11.05	11.15

TABLE VII. D-wave masses bottomonium $b\bar{b}$.

states	power index (p)	$R_{nl}(0)$ (GeV$^{3/2}$)	n^3D_1 (GeV)	n^3D_2 (GeV)	n^1D_2 (GeV)	n^3D_3 (GeV)
	0.1	0.081	10.170	10.171	10.171	10.172
	0.5	0.556	10.167	10.170	10.171	10.174
1D	1.0	1.195	10.165	10.170	10.171	10.175
	1.5	1.702	10.163	10.170	10.171	10.176
	2.0	2.257	10.160	10.169	10.171	10.178
	[6]		10.164	-	-	-
	[16]		10.135	10.141	10.142	10.146
	0.1	0.022	10.223	10.224	10.224	10.225
	0.5	0.228	10.363	10.367	10.369	10.372
2D	1.0	0.615	10.504	10.514	10.517	10.525
	1.5	1.110	10.610	10.627	10.632	10.646
	2.0	1.475	10.698	10.719	10.725	10.743

the pseudoscalar and vector states of $c\bar{c}$ and $b\bar{b}$ for different power index p, potential model parameter b is fitted .The potential model parameters used in the present work are shown in Table I.

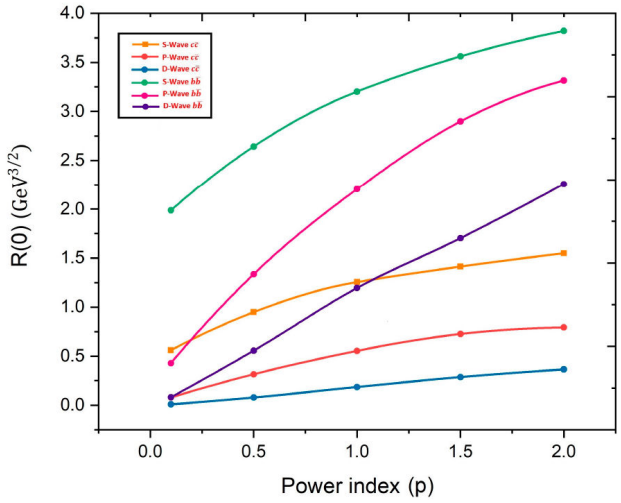

FIGURE 1. $R_{nl}(0)$ (GeV$^{3/2}$) → power index (p).

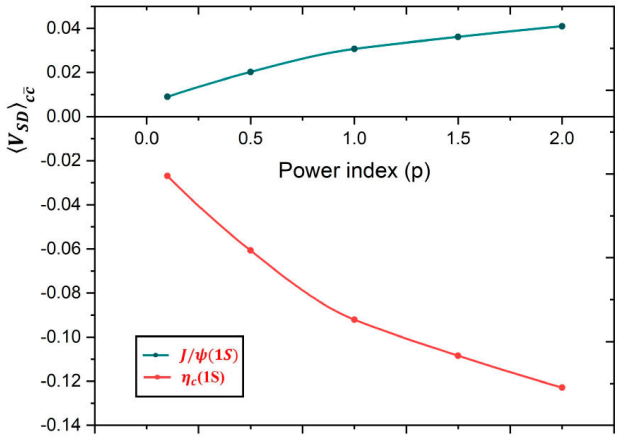

FIGURE 2. S-Wave $\langle V_{SD}\rangle_{c\bar{c}}$ → power index (p).

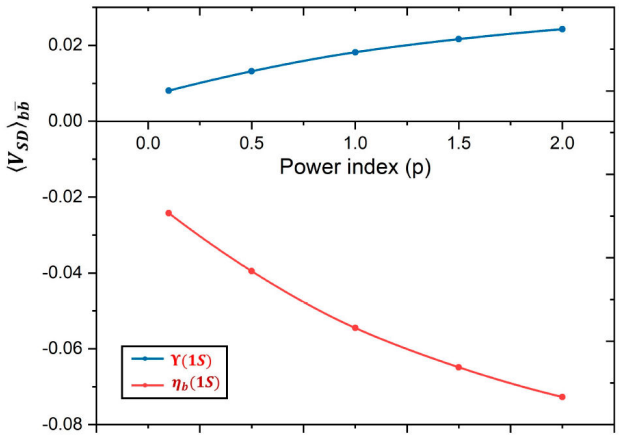

FIGURE 3. S-Wave $\langle V_{SD}\rangle_{b\bar{b}}$ → power index (P).

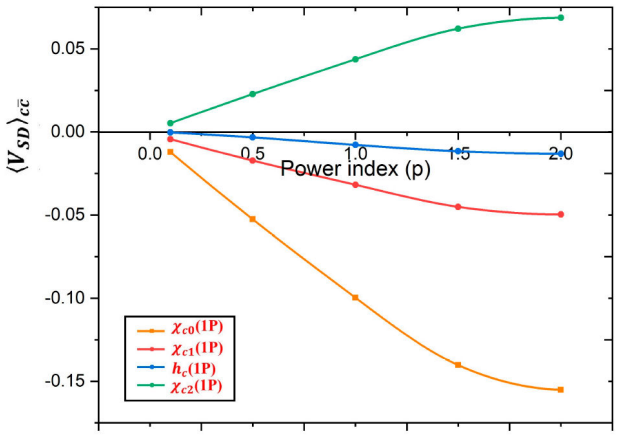

FIGURE 4. P-Wave $\langle V_{SD}\rangle_{c\bar{c}}$ → power index (p).

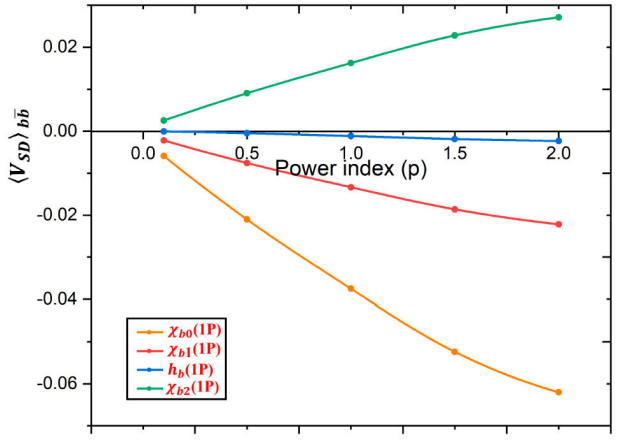

FIGURE 5. P-Wave $\langle V_{SD}\rangle_{b\bar{b}}$ → power index (p).

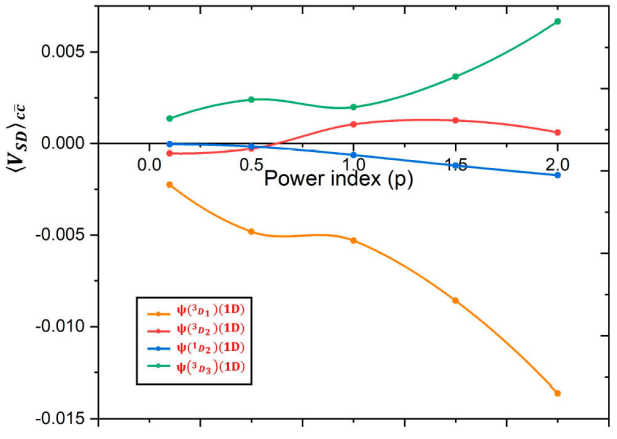

FIGURE 6. D-Wave $\langle V_{SD}\rangle_{c\bar{c}}$ → power index (p).

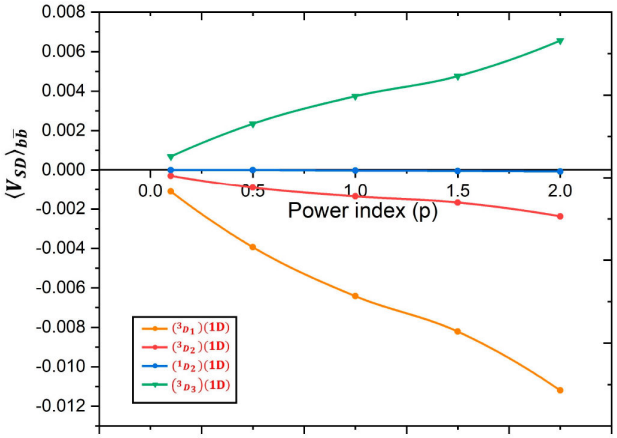

FIGURE 7. D-Wave $\langle V_{SD}\rangle_{b\bar{b}} \rightarrow$ power index (p).

The mass spectra of the nS, nP and nD states of charmonium $(c\bar{c})$ and bottomonium $(b\bar{b})$ are tabulated in Tables II - VII. The consistency and reliability of our theoretical model have been tested by comparing the mass spectra of charmonium $(c\bar{c})$ and bottomonium $(b\bar{b})$ with experimental results available in recent PDG [6] as well as masses predicted by other available theoretical model such as non-relativistic quark model and Relativistic quark model.

In Fig. 1, we have plotted the radial wave function at origin for the charmonium $R_{c\bar{c}}(0)$ as well as bottomonium $R_{b\bar{b}}$ with variation of power index p. It can be seen that the radial wave function at origin in both system, charmonium $R_{c\bar{c}}(0)$ and bottomonium $R_{b\bar{b}}(0)$ increases with increase of power index p. In order to examine the effect of the spin-spin (V_{SS}), spin-orbit (V_{LS}), and spin-tensor(V_T) interactions on the masses and decay-widths of heavy-flavour mesons with variation of the power index p, We have plotted the graph that shows the behaviour of the total spin dependent potential $\langle V_{SD}\rangle$ (the sum of the spin-spin, spin-orbit, and spin-tensor interaction potentials) with variation of power index p for S-wave, P-wave, and D-wave heavy flavour mesons shown in Figs. 2-7. From the graph it can be seen that the total spin dependent potential is gradually increases or decreases depending on the respective states of heavy flavour mesons.

3.2. Regge trajectories

We have plotted the Regge trajectories for the (J, M^2) and (n, M^2) planes with the help of masses estimated by our potential model. The daughter trajectories are the trajectories with same J^{PC} (P=parity , C= charge conjugation) value and differ by the corresponding radial principal quantum number n. The masses of the daughter trajectories are higher than the corresponding leading trajectories with given quantum numbers. The linear nature of Regge trajectories represents a reflection of a strong interactions between quarks [18]. The Regge trajectories in the (J, M^2) plane with natural parity $J^{PC} = 1^{--}, 2^{++}, 3^{--}, 4^{++}$ and unnatural parity $J^{PC} = 0^{-+}, 1^{+-}, 2^{-+}, 3^{+-}$ for charmonium $(c\bar{c})$ and bottomonium $(b\bar{b})$ are plotted in Fig. 8-11. The Regge trajectories for the (n_r, M^2) plane where $n_r = n - 1$ with principal quantum number n for charmonium and bottomonium are shown in Fig. 11-12. The fitted slopes (α, β) and intercepts (α_0, β_0) of the Regge trajectories for (J, M^2) and (n, M^2) planes are tabulated in the Tables VIII-XI are calculated by the following defination,

$$J = \alpha M^2 + \alpha_0, \tag{23}$$

$$n_r = \beta M^2 + \beta_0. \tag{24}$$

The estimated masses of the charmonium and bottomonium fit well to the (J, M^2) and (n, M^2) planes trajectories.

TABLE VIII. Slopes and intercepts of the (J, M^2) Regge trajectories for charmonium $(c\bar{c})$ states with unnatural and natural parity.

Parity	trajectory	slopes (α) (GeV^{-2})	intercepts (α_0)
unnatural	Parent	0.41 ± 0.07	-3.03 ± 0.88
	first daughter	0.45 ± 0.11	-5.20 ± 1.82
	second daughter	0.40 ± 0.07	-5.98 ± 1.57
natural	Parent	0.36 ± 0.05	-3.25 ± 0.67
	first daughter	0.45 ± 0.04	-6.09 ± 0.76
	second daughter	0.48 ± 0.02	-8.17 ± 0.45

TABLE IX. Slopes and intercepts of the (J, M^2) Regge trajectories for bottomonium $(b\bar{b})$ states with unnatural and natural parity.

Parity	trajectory	slopes (α) (GeV^{-2})	intercepts (α_0)
unnatural	Parent	0.12 ± 0.02	-11.34 ± 2.01
	first daughter	0.17 ± 0.01	-16.95 ± 2.01
	second daughter	0.19 ± 0.01	-20.27 ± 0.91
natural	Parent	0.14 ± 0.02	-11.61 ± 1.94
	first daughter	0.18 ± 0.01	-17.46 ± 1.49
	second daughter	0.18 ± 0.01	-18.67 ± 0.94

TABLE X. Slopes and intercepts of the (n_r, M^2) Regge trajectories for charmonium $(c\bar{c})$ states.

meson	J^{pc}	slopes (β) (GeV^{-2})	intercepts (β_0)
η_c	0^{-+}	0.265 ± 0.013	-2.422 ± 0.197
J/ψ	1^{--}	0.281 ± 0.009	-2.748 ± 0.156
χ_{c0}	0^{++}	0.363 ± 0.016	-4.258 ± 0.230
χ_{c1}	1^{++}	0.314 ± 0.011	-3.827 ± 0.168
h_c	1^{+-}	0.293 ± 0.007	-3.609 ± 0.117
χ_{c2}	2^{++}	0.263 ± 0.007	-3.345 ± 0.118
$\psi(^3D_1)$	1^{--}	0.317 ± 0.000	-4.513 ± 0.000
$\psi(^3D_2)$	2^{--}	0.299 ± 0.000	-4.271 ± 0.000
$\psi(^1D_2)$	2^{-+}	0.298 ± 0.000	-4.259 ± 0.000
$\psi(^3D_3)$	3^{--}	0.284 ± 0.000	-4.058 ± 0.000

TABLE XI. Slopes and intercepts of the (n_r, M^2) Regge trajectories for bottomonium $(b\bar{b})$ states.

meson	J^{pc}	slopes (β) (GeV^{-2})	intercepts (β_0)
η_b	0^{-+}	0.107 ± 0.013	-9.545 ± 1.228
Υ	1^{--}	0.126 ± 0.012	-11.48 ± 0.235
χ_{b0}	0^{++}	0.148 ± 0.009	-14.43 ± 0.939
χ_{b1}	1^{++}	0.142 ± 0.006	-13.91 ± 0.686
h_b	1^{+-}	0.140 ± 0.007	-13.76 ± 0.767
χ_{b2}	2^{++}	0.135 ± 0.004	-13.34 ± 0.515
$\Upsilon(^3D_1)$	1^{--}	0.142 ± 0.000	-14.73 ± 0.000
$\Upsilon(^3D_2)$	2^{--}	0.139 ± 0.000	-14.45 ± 0.000
$\Upsilon(^1D_2)$	2^{-+}	0.139 ± 0.000	-14.44 ± 0.000
$\Upsilon(^3D_3)$	3^{--}	0.138 ± 0.000	-14.29 ± 0.000

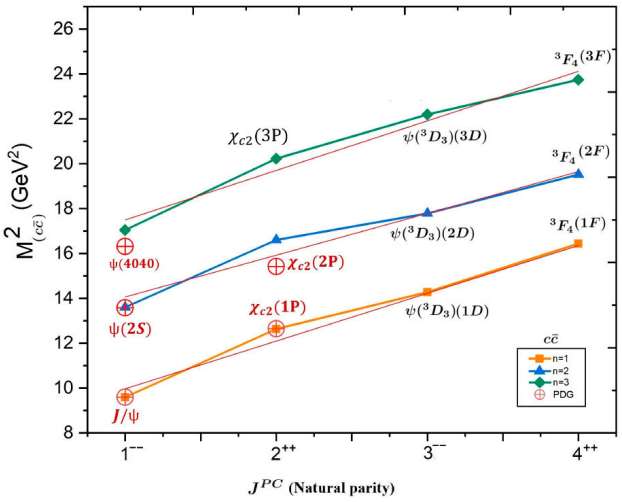

FIGURE 8. $M^2_{c\bar{c}}$ (GeV^2)$\rightarrow$ J^{PC} (Natural parity).

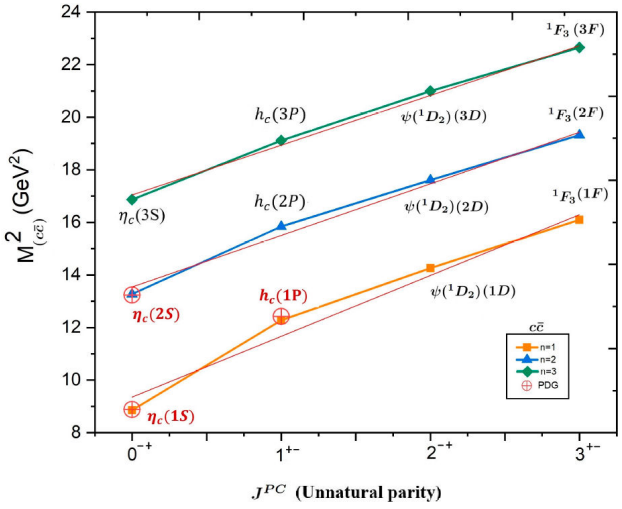

FIGURE 9. $M^2_{c\bar{c}}$ (GeV^2)$\rightarrow$ J^{PC} (Unnatural parity).

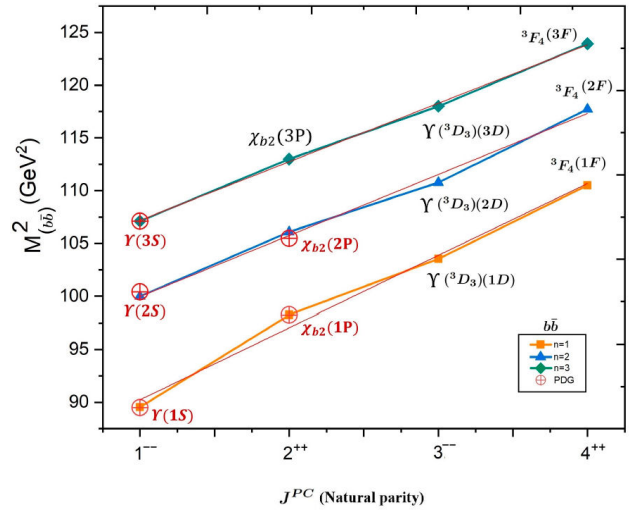

FIGURE 10. $M^2_{b\bar{b}}$ (GeV^2)$\rightarrow$ J^{PC} (Natural parity).

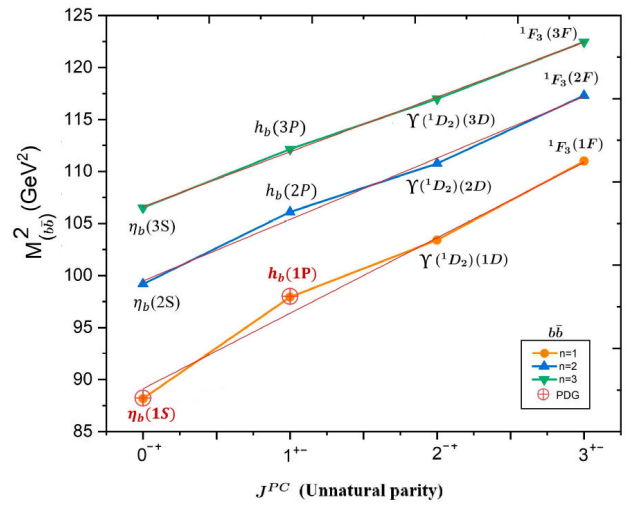

FIGURE 11. $M^2_{b\bar{b}}$ (GeV^2)$\rightarrow$ J^{PC} (Unnatural parity).

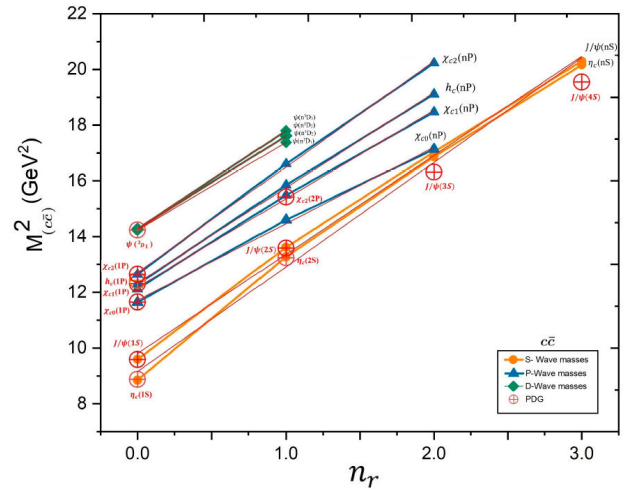

FIGURE 12. $M^2_{c\bar{c}}$ (GeV^2)$\rightarrow$ n_r.

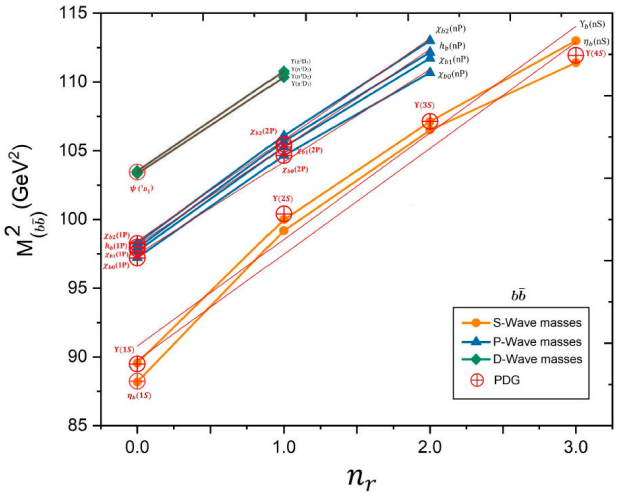

FIGURE 13. $M^2_{b\bar{b}}$ (GeV^2)$\rightarrow n_r$.

3.3. Decay properties

We have estimated the leptonic, photonic and gluonic decay widths of $c\bar{c}$ and $b\bar{b}$ decays into e^+e^-, two photon $(\gamma\gamma)$, three photon $(\gamma\gamma\gamma)$, two gluon (gg), three gluon$(3g)$, and γgg with and without QCD correction factor with the help of our potential model parameters, masses and respective radial wave function at the origin. Our results of the leptonic decay widths $\Gamma(n^3S_1 \rightarrow e^+e^-)$ of J/ψ and Υ decays into leptons e^+e^- for potential index p varying from 0.1 to 2.0 with and without QCD correction factor compared with other available theoretical as well as experimental results were shown in Table XII. It can be seen that the predicted leptonic decay width by other theoretical models are in agreement with experimental result upto 0.74-34.7% variations, while our predicted leptonic decay width with radiative quantum chromo-dynamics (QCD) correction factor at potential index $p = 1$ is in agreement with experimental result with 4.17-10.1% variations. In Fig. 14, we have plotted the leptonic decay width with variation of the power index p.From the graph it is observed that the predicted leptonic decay widths increases monotonously and slowly with increase of the power index p.Our results of the two photonic decay widths $\Gamma(n^1S_0 \rightarrow \gamma\gamma)$ of η_c and η_b decays into two photons and $\Gamma(n^3S_1 \rightarrow \gamma\gamma\gamma)$ of J/ψ and Υ decays into three photons were shown in Table XIII and XIV respectively. It can be seen that the predicted photonic decay width by other theoretical models are in agreement with experimental result upto 29-55% variations, while our predicted photonic decay width with radiative quantum chromodynamics (QCD) correction factor at potential index $p = 1$ is in agreement with experimental result with 5.01-6.29% variations. In Fig. 15 and 16, we have plotted the photonic decay width of charmonium and bottomonium with variation of the power index p repectively. From the graph it is observed that the predicted photonic decay widths increases monotoeously with increase of the power index p.Our results of the two gluonic decay widths $\Gamma(n^1S_0 \rightarrow gg)$ of η_c and η_b decays into two gluons, $\Gamma(n^3S_1 \rightarrow ggg)$ and $\Gamma(n^3S_1 \rightarrow \gamma gg)$ of J/ψ and Υ decays into three gluons and γgg were shown in Table XV, XVI and XVII respectively. It can be seen that the predicted gluonic decay width by other theoretical models are in agreement with experimental result upto 9.89-54.3% variations, while our predicted gluonic decay width with radiative quantum chromo-dynamics (QCD) correction factor at potential index $p = 1$ is in agreement with experimental result with 2.58-3.71% variations. In Fig. 17 and 18, we have plotted the gluonic decay width of charmonium and bottomonium with variation of the power index p respectively . From the graph it is observed that the predicted gluonic decay widths increases monotoeously with increase of the power index p.

We can conclude that our results of mass spectra of charmonium and bottomonium (Table II-VII) predicted using a color coulomb plus confinment power law potential with variation of power index p from 0.1 to 2, are in good accordance with the available experimental as well as predicted by other theoretical models at power index $p = 1$. We observe from the Regge trajectories in the (J, M^2) and (n, M^2) plane (Figure 8-13) that the experimental masses of charmonium states and bottomonium states are sitting nicely on the trajectories. In the mass region of the lowest excitations of charmonium and bottomonium, the slopes as well as The curvature of the trajectories decreases with increasing quarkonium masses. The results of annihilation decay widths of leptonic, photonic and gluonic decays of charmonium and bottomonium (Table XII-XVII) with using QCD correction factor are in good aaccordance with the available experimental results at power index $p = 1$. Hence, the overall results of the mass spectra, Regge trajectories and decay widths of heavy-flavour mesons predicted by our theoretical model are in good accordance with the available experimental as well as predicted by other theoretical models at power index $p = 1$.

TABLE XII. Leptonic decay widths $\Gamma(n^3S_1 \rightarrow e^+e^-)$ in keV.

power	$\Gamma(J/\psi \rightarrow e^+e^-)$				$\Gamma(\Upsilon \rightarrow e^+e^-)$			
index	present work		other work		present work		other work	
(p)	$\Gamma^{e^+e^-}$	$\Gamma^{e^+e^-}_{cf}$	$\Gamma^{e^+e^-}_{th}$	$\Gamma^{e^+e^-}_{exp}$	$\Gamma^{e^+e^-}$	$\Gamma^{e^+e^-}_{cf}$	$\Gamma^{e^+e^-}_{th}$	$\Gamma^{e^+e^-}_{exp}$
0.1	3.137	1.006	4.280 [17]	5.55 [6]	1.047	0.547	0.710 [12]	1.340 [6]
0.5	8.926	2.864	3.623 [18]		1.897	0.991	1.330 [17]	
1.0	15.55	4.992			2.711	1.396		
1.5	19.61	6.294			3.455	1.805		
2.0	23.52	7.356			3.896	2.036		

TABLE XIII. Two-Photonic decay widths $\Gamma(n^1S_0 \to \gamma\gamma)$ in keV.

	$\Gamma(\eta_c \to \gamma\gamma)$				$\Gamma(\eta_b \to \gamma\gamma)$			
Power	present work		other work		present work		other work	
index(p)	$\Gamma^{\gamma\gamma}$	$\Gamma^{\gamma\gamma}_{cf}$	$\Gamma^{\gamma\gamma}_{th}$	$\Gamma^{\gamma\gamma}_{\rm exp}$	$\Gamma^{\gamma\gamma}$	$\Gamma^{\gamma\gamma}_{\rm cf}$	$\Gamma^{\gamma\gamma}_{\rm th}$	$\Gamma^{\gamma\gamma}_{\rm exp}$
0.1	1.070	0.923	6.62 [18]	5.1 [6]	0.359	0.225	0.690 [12]	-
0.5	3.140	2.707	7.91 [19]		0.651	0.409	0.730 [19]	
1.0	5.618	4.844			0.932	0.585		
1.5	7.194	6.202			1.188	0.746		
2.0	8.740	7.536			1.341	0.842		

TABLE XIV. Three-photonic decay widths $\Gamma(n^3S_1 \to \gamma\gamma\gamma)$ in eV.

	$\Gamma(J/\psi \to \gamma\gamma\gamma)$				$\Gamma(\Upsilon \to \gamma\gamma\gamma)$			
Power	present work		other work		present work		other work	
index(p)	$\Gamma^{\gamma\gamma\gamma}$	$\Gamma^{\gamma\gamma\gamma}_{cf}$	$\Gamma^{\gamma\gamma\gamma}_{th}$	$\Gamma^{\gamma\gamma\gamma}_{exp}$	$\Gamma^{\gamma\gamma\gamma}$	$\Gamma^{\gamma\gamma\gamma}_{cf}$	$\Gamma^{\gamma\gamma\gamma}_{th}$	$\Gamma^{\gamma\gamma\gamma}_{exp}$
0.1	0.417	0.204	3.94 [18]	1.08 [6]	0.871	0.563	3.440 [12]	-
0.5	1.187	0.581			1.577	1.020		
1.0	2.069	1.012			2.254	1.457		
1.5	2.609	1.276			2.872	1.857		
2.0	3.129	1.531			3.240	2.095		

TABLE XV. Two-Gluonic decay widths $\Gamma(n^1S_0 \to gg)$ in MeV.

	$\Gamma(\eta_c \to gg)$				$\Gamma(\eta_b \to gg)$			
Power	present work		other work		present work		other work	
index(p)	Γ^{gg}	Γ^{gg}_{cf}	Γ^{gg}_{th}	Γ^{gg}_{exp}	Γ^{gg}	Γ^{gg}_{cf}	Γ^{gg}_{th}	Γ^{gg}_{exp}
0.1	3.617	5.643	36.58 [18]	28.6 [6]	10.93	13.37	20.18 [12]	-
0.5	10.60	16.55	13.07 [19]		19.81	11.48	10.86 [19]	
1.0	18.98	29.61			28.34	16.43		
1.5	24.30	37.92			36.15	20.96		
2.0	29.52	46.07			40.78	23.65		

TABLE XVI. Three-Gluonic decay widths $\Gamma(n^3S_1 \to ggg)$ in KeV.

	$\Gamma(J/\psi \to ggg)$				$\Gamma(\Upsilon \to ggg)$			
Power	present work		other work		present work		other work	
index(p)	Γ^{ggg}	Γ^{ggg}_{cf}	Γ^{ggg}_{th}	$\Gamma^{ggg}_{\rm exp}$	Γ^{ggg}	Γ^{ggg}_{cf}	Γ^{ggg}_{th}	$\Gamma^{ggg}_{\rm exp}$
0.1	72.44	11.56	269.1 [18]	59.55 [6]	40.82	21.72	-	-
0.5	206.1	32.91			73.93	39.33		
1.0	359.1	57.34			105.6	56.20		
1.5	452.8	72.30			134.6	71.63		
2.0	543.2	86.73			151.8	80.79		

TABLE XVII. Decay widths of $\Gamma(n^3S_1 \to \gamma gg)$ in keV.

	$\Gamma(J/\psi \to \gamma gg$				$\Gamma(\Upsilon \to \gamma gg)$			
power	present work		other work		present work		other work	
index (p)	$\Gamma^{\gamma gg}$	$\Gamma^{\gamma gg}_{\rm cf}$	$\Gamma^{\gamma gg}_{\rm th}$	$\Gamma^{\gamma gg}_{\rm exp}$	$\Gamma^{\gamma gg}$	$\Gamma^{\gamma gg}_{\rm cf}$	$\Gamma^{\gamma gg}_{\rm th}$	$\Gamma^{\gamma gg}_{\rm exp}$
0.1	4.230	1.860	8.1 [18]	8.99 [6]	0.794	0.506	-	-
0.5	12.03	5.293			1.439	0.917		
1.0	20.97	9.222			2.056	1.310		
1.5	26.44	11.62			2.621	1.669		
2.0	31.72	13.95			2.955	1.883		

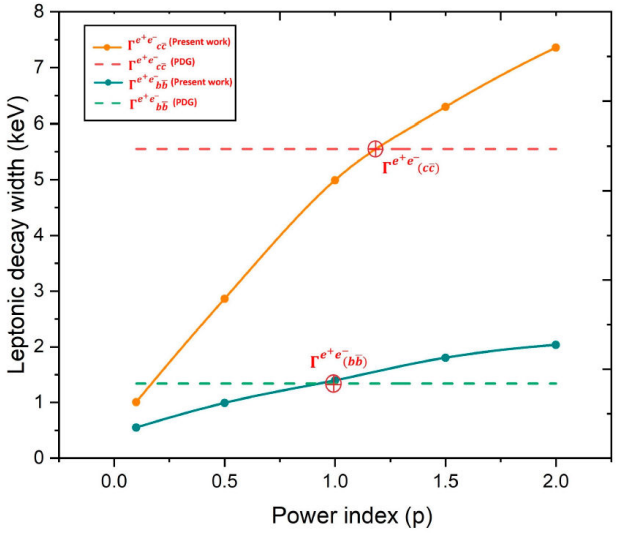

FIGURE 14. Leptonic decay width → power index (p).

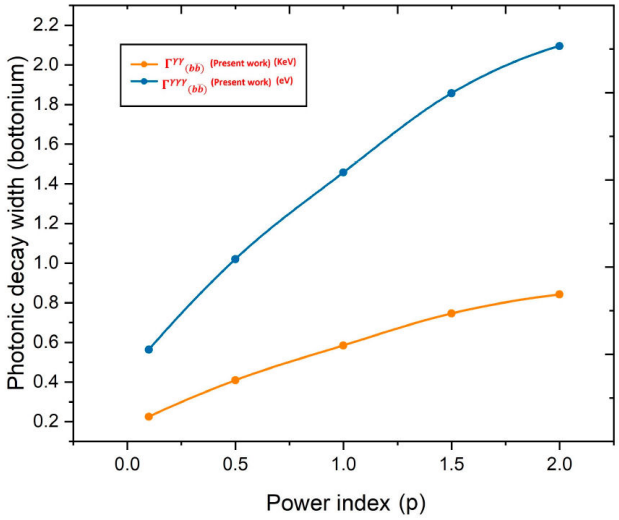

FIGURE 16. Photonic decay width (bottomonium)→ power index (p).

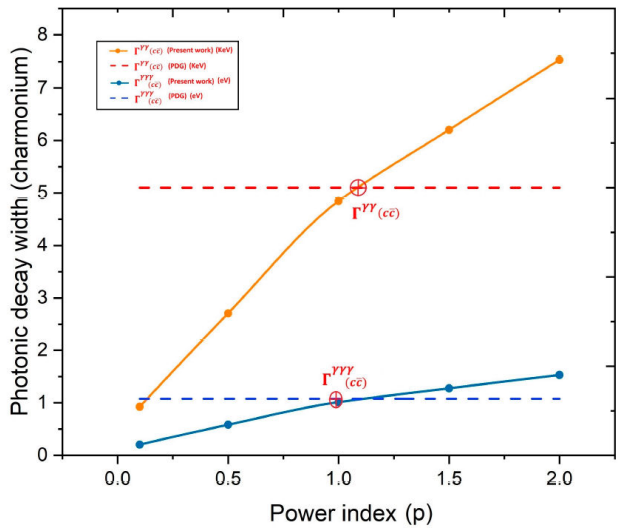

FIGURE 15. Photonic decay width (charmonium) → power index (p).

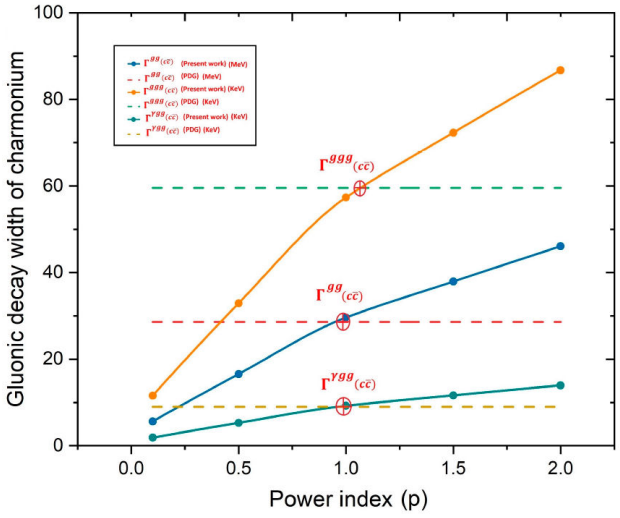

FIGURE 17. Gluonic decay width (charmonium) → power index (p).

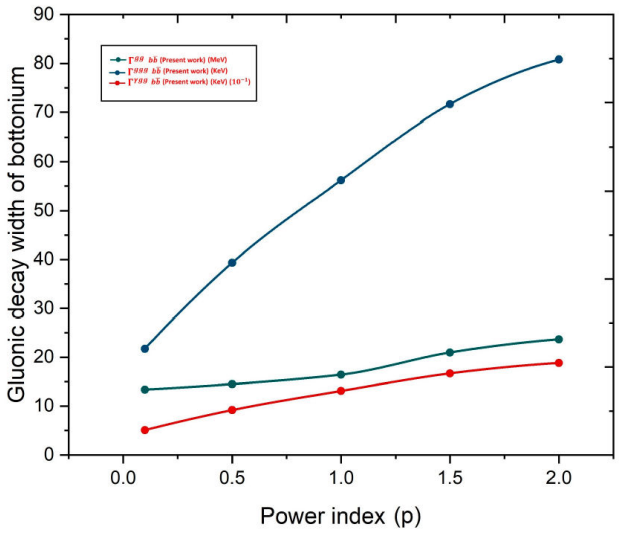

FIGURE 18. Gluonic decay width (bottomonium) → power index (p).

1. J.J. Aubert *et al*., *Phys. Rev. Lett* **33** (1974) 1404.
2. J. E. Augustine *et al*., *Phys. Rev. Lett* **33** (1974) 1406.
3. S. Herb *et al*., *Phys. Rev. Lett*. 39 (1977) 252.
4. W. R. Innes *et al*., *Phys. Rev. Lett*. 39 (1977) 1240.
5. G. Goldhaber *et al*., *Phys. Rev. Lett* **37** (1976) 255.
6. Particle Data Group *et al.*, **2020** (2020) 083C01.
7. W. Kwong, P. B. Mackenzie, R. Rosenfeld, and J. L. Rosner, *Phys. Rev. D* **37** (1988) 3210.
8. W. Kwong, and J. L. Rosner, *Phys. Rev. D* **38** (1988) 279.
9. W. Lucha *et al*., Effective potential models for hadrons HEPHY-PUB 621/95 (1995).
10. R. Mistry, and A. Majethiya, Branching ratios and decay widths of the main, hidden and open charm channels of tetraquark states. *Eur. Phys. J. A* **59** (2023) 107.
11. H A Bethe and E E Salpether Quantum Mechanics of atoms of one-and two-electrons Springer (1957)
12. J. Segovia, P.G. Ortega, D.R. Entem, F. Fernndez, *Phys. Rev. D* **93** (2016) 074027.
13. A. Bradley, A. Khare, *Z. Phys. C* **8** (1981) 131.
14. G. Belanger, P. Moxhay, *Phys. Lett. B* **199** (1987) 575.
15. R. Tiwari, D. P. Rathaud, and A. K. Rai, Spectroscopy of all charm tetraquark states. *Indian J Phys* **97** (2023) 943-954.
16. R. Tiwari, D. P. Rathaud, and A. K. Rai, *Eur. Phys. J. A* **57** (2021) 289.
17. S. F. Radford and W. W. Repko, *Phys. Rev. D* **75** (2007) 074031.
18. V. Kher and A. Kumar Rai, *Chinese Phys. C* **42** (2018) 083101.
19. H. Negash, S. Bhatnagar, *Int. J. Mod. Phys. E* **25** (2016) 1650059.